SPE/ISRM 47212

IN-SITU STRESS AND PORE PRESSURE IN THE SOUTH EUGENE ISLAND FIELD, GULF OF MEXICO

T. Finkbeiner and M.D. Zoback, SPE, Department of Geophysics, Stanford University

This paper was prepared for presentation at SPE/ISRM Eurock '98 held in Trondheim, Norway, 8–10 July 1998.

Abstract

Analysis of minifracs and pore pressure surveys from sand reservoirs in a Gulf of Mexico oil field show effective stress ratios, K, that scatter significantly and do not correlate with previously published fracture gradient models for this area. The lower-bound value of K is 0.33, which corresponds to the expected value for Coulomb failure for a coefficient of friction of 0.6 in normal faulting environments. However, in some sands K approaches unity, thus indicating an essentially isotropic stress field. Hence, the data indicate a highly variable state of stress that cannot be simply related to depth or pore pressure, but appears to reflect an interaction between deformational processes and material properties.

Borehole breakout analysis in vertical wells reveals stress orientations that are predominantly perpendicular to normal faults and, hence, consistent with an extensional stress regime. Analysis of breakouts in inclined wells in two sand reservoirs allows to constrain the magnitude of the maximum horizontal principal stress, S_{Hmax}, and further indicates an active normal faulting environment with a clear, but small degree of horizontal stress anisotropy (i.e., $S_V > S_{Hmax} > S_{hmin}$).

Introduction

Determination of the full stress tensor in oil fields is critical for addressing engineering issues such as borehole stability and sand production as well as understanding dynamic constraints on hydrocarbon migration and fracture permeability.

In this study we use data from minifracs, pore pressure surveys, and dipmeter caliper logs to constrain the full in-situ stress tensor (i.e., the magnitude and orientation of all three principal stresses) in reservoirs sands from the South Eugene Island (SEI). This field is located in the Gulf of Mexico on the outer continental shelf about 100 miles offshore Louisiana. Geologically, this field is a "classical" Plio-Pleistocene Gulf of Mexico salt-withdrawal minibasin that is bounded to the north and east by a regional (down to the south) fault system and to the south by an antithetic fault system[1]. Over 25 unconsolidated sands layers are separated by massive shale packages and normal faults into at least 100 structurally or stratigraphically distinct reservoirs. The field is one of the largest oil and gas producing fields in the US[2,3]. As the hydrocarbons trapped within the reservoirs of SEI field are much older than the young sediments, they are believed to have migrated vertically over significant distances relatively recently[2]. **Fig. 1** displays a schematic N-s trending cross-section through the field showing the main basin bounding growth fault system in the middle as it offsets sand reservoirs in the footwall (to the right) from those in the hanging wall (to the left). Note, that the structural relief across the fault system increases significantly with depth while individual sand reservoirs become less continuous.

The availability of minifrac data from fracture completions and pore pressure history data from pressure surveys from the SEI field provides an unique opportunity to accurately characterize in-situ least principal stresses and pore pressures in the hydrocarbon producing sand reservoirs. Integrating these least principal stress measurements with carefully analyzed pore pressure data and borehole breakouts from dipmeter caliper data in vertical and inclined wells allows us to constrain the full stress tensor in these reservoir sands and to compare with published estimates of the least principal stress derived from fracture gradients. There are three clear advantages of this study over previous studies of this type in the Gulf coast region: (1) We can use least principal stress data from minifracs conducted in sands whereas previous studies derived stress data from low quality leak-off tests that were predominantly measured in shales. (2) Our stress measurements were taken in the same reservoir sands in which pore pressures were measured whereas previous compilations often compare stress data from shales with pore pressure data from sands. (3) All of our data come from the same field (and often even the same well) whereas previous publications reflect regional compilations.

Pore pressure history data from numerous production wells also allow us to quantify production related pore pressure

drawdown and stress changes. Since many of the minifracs were carried out in reservoirs sands that showed significant pore pressure decline, we anticipated associated stress changes due to poroelastic effects.

Least Principal Stress and Pore Pressure

Twenty fracture completions from 17 production wells within the SEI 330 field provided least principal stresses data from fracture completions. We chose the minifrac bottomhole closure pressure to be the closest value to the least principal stress ($S_3 = S_{hmin}$). Pore pressure values are generally measured before the minifracture test after perforation. We quality controlled these values with pore pressure history records, which were in good agreement and required only few minor adjustments. The values for the vertical stress, S_V, were calculated by integrating bulk-density logs to the depths of perforation.

Results. Initial (i.e., undepleted) reservoir pore pressures and stresses varied considerably in the reservoir sands of the SEI field. Pore pressure values (i.e., $\lambda = P_p/S_V$) ranged from near hydrostatic ($\lambda = 0.48$) to $\lambda = 0.95$ of the vertical stress and least principal stresses from $\lambda = 0.8$ to $\lambda = 0.99$. In the following, we display our data in two different ways that allow us to quantify the state of stress in the reservoir sands and compare them with widely accepted fracture gradient predictions from the literature.

Stress and Pore Pressure Variations Versus Depth. **Fig. 2** shows reservoir conditions from sands within the minibasin and the footwall (Fig. 1). In this case, we display pore pressures and stresses versus depth for both depleted (open symbols) and restored (i.e., initial, solid symbols) conditions using the methodology described below. In Fig. 2a, we demonstrate the effect of drawdown and the applied pore pressure correction for all reservoirs studied. Note, for some sands the drawdown was negligible resulting in partial or complete overlay of the symbols. In other sands we find that the production related drawdown has been significant resulting, in two cases, to even sub-hydrostatic pore pressures. In the undepleted reservoirs (i.e., initial conditions, black triangles), λ increases with depth from mildly to severely overpressured (i.e., $0.5<\lambda<0.95$) and follows one of two pore pressure trends depending on whether the measurements were taken in a minibasin or footwall reservoir. In Fig. 2b we converted our data to effective stress ratio, K. This ratio is calculated by simply taking the ratio of the effective least horizontal stress, σ_{hmin} ($S_{hmin} - P_p$), over the effective overburden stress, σ_V ($S_V - P_p$):

$$K = \sigma_{hmin}/\sigma_V. \quad \text{..... (2)}$$

In general, it is assumed that K shows a clear trend in the sense that it increases with depth[4,5,6,7,8]. In contrast, our data show no clear correlation but rather scatter, regardless whether we consider depleted (open triangles) or initial (black and gray triangles) conditions. For the initial state we find that K is limited by two bounds: (1) $K = 0.32$ and (2) $K = 1$. The first value corresponds to frictional faulting theory (i.e., Coulomb failure criterion) for a coefficient of friction (μ) of 0.6:

$$K = \sigma_{hmin}/\sigma_V = [(\mu^2+1)^{0.5}+\mu]^{-2}. \quad \text{..... (3)}$$

According to this model, the state of stress is in frictional equilibrium with pre-existing, optimally oriented shear planes and faults[9]. The second value relates to an isotropic stress state in which all differential stresses in the reservoir sands have dissipated comparable to an ideal fluid. $K = 1$ is also the upper bound in a region of normal faulting where the overburden, S_V, is the maximum principal stress.

Least Principal Horizontal Stress Versus Pore Pressure. In **Fig. 3** we display our data in normalized stress/pore pressure space (i.e., normalized by S_V). Again, we show depleted (open triangles) and initial (black triangles) conditions. This dimensionless plot removes any explicit depth effect and allows us to directly compare all stress measurements amongst themselves and with three published fracture gradient predictions[4,5,6], which we consider representative of most regressions published in the literature. In addition, the figure exhibits the fracture gradient regression from Pennzoil for the SEI field (unpublished, black line with dots) and three rock mechanical failure lines: (1) the hydrofrac failure limit at which the pore pressure equals the least principal stress and natural hydraulic fracturing[10] occurs, (2) frictional failure[9] for $\mu = 0.6$ for which $K = 0.32$, (3) the isotropic stress state for which $K = 1$. Note, that the lines for natural hydraulic fracturing and frictional failure for $\mu = 0.6$ converge as the pore pressure increases.

Again, the figure shows that the stresses and pore pressures in these sands are such that they can be bound by frictional failure for $\mu = 0.6$ and an isotropic stress state. This observation suggests that frictional equilibrium may act as a lower bound for the least principal stress in this normal faulting environment. Two-thirds of the reservoirs show pore pressure and stress conditions that are above the lower bound. We can deduce that their S_{hmin} values are higher than predicted by Coulomb failure for $\mu = 0.6$ because they exhibit lower differential stresses. Laboratory experiments by Chang and Zoback[11] have shown that unconsolidated sands from SEI relax visco-elastically and dissipate differential stresses. Other possibilities to explain our observations include that these reservoir sands are not at failure or they are mechanically weaker and only support small shear stresses (i.e., the coefficient of friction is appreciably lower than 0.6).

Comparing our South Eugene Island data with three common fracture gradient regressions from the Gulf of Mexico[4,5,6] (Fig. 4) demonstrates that there is no obvious correlation with either the depleted or the initial pore pressures and stresses. We think this mismatch is a result of our stress and pore pressure data being exclusively from within sand reservoirs in one specific Gulf Coast field; the three representative compilations, in contrast, are empirical regressions based on regional stress data from shales. In fact, for most of our data points the regressions overpredict the stress magnitudes (i.e., S_{hmin}) in the sands, which is in agreement with the idea that stresses in shales are generally higher.

However, there is also no obvious match among the regressions themselves. We attribute this to the fact that they are not only based on various regional data but also on different data types for stress determination. For example,

Breckels and vanEekelen[5] primarily used formation integrity tests (FITs), which are ambiguous for least principal stress determination since the reservoir is not fractured. Althaus[4] and Brennan and Annis[6] used circulation losses and leak-off tests (LOTs) respectively. While these tests usually cause the sedimentary rock to fail, it is not clear whether they reflect the breakdown, propagation, closure, or some intermittent pressure, which can be very different.

In summary, we think the regressions prove not to be useful in predicting least principal stresses in sand reservoirs of the SEI field. Regardless of whether we consider depleted or initial (i.e., drawdown corrected) conditions, our data exhibit significant scatter which implies that stresses in these reservoir sands cannot be related to depth or pore pressure by a simple relation. The data rather reflect a complex interaction between deformational processes (i.e., varying stress/strain boundary conditions) and material properties.

Drawdown Correction. Because more than half of the reservoirs had experienced significant depletion by the time of fracture completion, many of the S_{hmin} value measured do not reflect the unperturbed state of stress in the field and needs to be restored. Estimating the change of least principal stress with the change of pore pressure (i.e., the stresspath) is generally a difficult task, especially for poorly consolidated sediments such as those of the SEI field (which potentially behave plastically when they compact). To bypass the problem of assuming a constitutive compaction law for these soft sediments[12], we carefully searched leak-off test (LOT) data from wells drilled into initially undepleted reservoir sands. The difference of this stress magnitude with the S_{hmin} value from the minifrac carried out at a time when the reservoir had been produced quantifies the change of least principal stress, ΔS_{hmin}. We obtained the associated reservoir pore pressure change, ΔP_p, from the pore pressure surveys. Given the two values for ΔP_p and ΔS_{hmin} we can define the stress path parameter A as

$$A = \Delta S_{hmin}/\Delta P_p \quad \text{..... (1)}$$

Parameter A presents the effective reservoir behavior under loading conditions (i.e., increase of effective stress as the pore pressure is drawndown) and reservoir rheology. Note, that A does not impose any boundary conditions on the physical behavior of the reservoir. Because we consider only two points along this stress path (initial state and depleted state at some later time), any intermittent time or pressure dependent compaction behavior is averaged out and the actual stress path of the reservoir is neglected.

From our LOT data, we were able to identify one LOT that was carried out in a reservoir sand and clearly fractured the formation. In **Fig. 4** we display changes of reservoir pore pressure (from pressure surveys in 6 different wells) and least principal stresses as a function of time and illustrate how we derive ΔP_p and ΔS_{hmin} in this particular reservoir sand. The resulting value for A is 0.81. This value is similar to results found by Engelder and Fischer[12] and Teufel et al. [13].

Because this is the only LOT we found in an undepleted reservoir of all the reservoirs studied, we assumed the same value for A (i.e., they follow the same stress path) for the remaining reservoir sands with significant drawdown history in order to restore their state of stress. While this may be a simplifying assumption we still prefer it over the odeometric compaction model for the reservoir sediments which imposes strict assumptions about elastic properties and boundary conditions.

One data point in Fig. 2b plots slightly to the right (K = 1.1) of the upper limit for K. We think that in this particular reservoir the value for A= 0.8 to restore the initial state of stress was probably somewhat too high (an isotropic stress state would be achieved for A= 0.7).

Full Stress Tensor Determination

Introduction. Stress-induced wellbore breakouts indicate stress orientation in the uppermost crust[14,15,16,17,18,19]. When the wellbore is nearly vertical (i.e., parallel to the vertical stress, S_V), breakouts form in the direction of the minimum principal horizontal stress (S_{hmin}), where stress concentrations at the borehole wall exceed the rock strength (C_0). Mechanisms that describe the formation of these features are discussed extensively in the literature[14,18,20]. In inclined wells, where the borehole axis is not parallel with any of the principal stresses, the location of the breakouts around the wellbore rotates and does not indicate the true orientation of S_{hmin}. Observation of these breakouts from various nearby wells, however, can be utilized to determine not only stress tensor orientation but also principal stress magnitudes[21,22].

Breakout Interpretation. In order to identify breakout intervals from caliper data, certain criteria have to be met which provide a means to distinguish them from other borehole enlargements such as washouts or key seat[23]. These two features are a result of the drilling process and occur frequently in inclined wells that penetrate poorly compacted and/or overpressured sediments such as the shales and sands encountered at depth in the SEI field. In particular key-seats are easily misinterpreted as breakouts since they occur due to pipewear at the high-side of the hole resulting in directional enlargements parallel to the hole-azimuth while the orthogonal caliper pair can remain in-gauge. For this reason, it is absolutely necessary to follow strict guidelines because misidentifications can lead to erroneous interpretations, hence, deceiving results for the state of stress.

Criteria. The criteria for interpreting an enlarged borehole interval as a breakout interval are as follows: (1) cessation of tool rotation; (2) steady and continuous enlargement of one caliper pair, while the second pair is in-gauge with the bitsize; (3) the enlarged caliper pair is not parallel with the hole-azimuth. The third point is particularly critical and requires careful analysis of the data because it helps to distinguish between breakouts and key seats.

Quality. Caliper logs from dipmeter data in 38 wells of the SEI field were the basis for our borehole breakout analysis. After filtering, all borehole enlargements through our selection criteria, we identified 70 borehole breakout intervals in 21 wells. We rank the quality of the selected breakouts to be fair or good because poor quality elongations would not pass

through our rigorous selection criteria described above.

While the observed breakout intervals occurred over a fairly wide depth range, it is important to note that breakouts also occurred in deep, severely overpressured sediments, where the state of stress is nearly isotropic. We believe this is a consequence of the extremely low rock strength because sediments cored from reservoirs at this level show essentially no cementation.

Stress Orientation. Depending on the inclination of the boreholes, there are two different ways to get the orientation of the stress tensor from wellbore breakout observations. (1) In near-vertical wells with inclinations less than 20°, breakout directions indicate directly the orientation of the least principal horizontal stress (S_{hmin}). We used breakout intervals observed in both sands and shales from (near-)vertical wells to obtain stress orientation because we think that in both lithologies stress orientations are more or less equivalent. (2) In highly deviated wells (i.e., inclinations greater than 20°) breakouts rotate away from the S_{hmin} direction[24] obscuring the true principal horizontal stress directions. However, stress orientation can be obtained from these breakouts given independent sources for S_{hmin} and P_p[21,22]. For this task, we used breakouts that were observed only in sand reservoirs, for which we also had independent and accurate pore pressure and stress data available. We address this issue in the next section.

Plotting the average stress orientations from each individual well on a structure map enables us to compare these with the general structure and the resulting stress orientation direction found in another study in the SEI field[22]. Note, that we assume that the overburden (S_V) is a principal stress axis. We think that this may be a reasonable assumption because vertical fractures were observed in the core[25] and formation micro imager (FMI) data[22] from the Pathfinder well, which is located in block 330 of the SEI field (Fig. 1).

Results. Because of the extremely variable geologic structures (both laterally and vertically), the presence of salt diapirs, and the spatially dispersed data throughout the field, we examine the resulting stress directions in three different structural levels: (1) the GA sand (4,150 ft. to 5,500 ft. SSTVD; hydrostatically pressured, $\lambda = P_p / S_V = 0.465$), (2) the LF sand (6,000 ft. to 7,600 ft. SSTVD; moderately overpressured, $\lambda = 0.64$), and (3) the Lentic sand (6,500 ft. to 11,200 ft. SSTVD; severely overpressured, $\lambda = 0.95$). The three structure maps in **Fig. 5** display the resulting stress directions obtained from breakouts in wells with less than 20° inclination in black and from breakouts in two wells with an inclination greater than 20° in gray (Lentic level, Fig. 5c). Note, the arrows point outwards in the direction of S_{hmin}, the azimuth of the mean breakout direction.

In the Lentic sand (Fig. 5c) the S_{hmin} directions in the two wells in block 330 and the vertical well in block 316 (black arrow) are perpendicular to normal faults as we would expect. In contrast, S_{hmin} in the inclined well in block 316 (labeled "12", gray arrow) is almost at 90° from the nearby vertical well (black arrow in block 316) and parallels an antithetic normal fault. It remains unclear to us why there exists such a discrepancy in the orientation of S_{hmin} between the two proximal wells in block 316 given their similar stratigraphy and pore pressure conditions. One explanation could be the near isotropic state of stress in this severely overpressured environment that allows localized stress perturbations to be responsible for seemingly random breakout orientations.

In the intermediate LF sand (Fig. 5b) three of the wells exhibit S_{hmin} directions that are (sub-)perpendicular to the nearest normal fault, which is in agreement with our expectations. In block 338, the stress orientation in the well that is furthest to the west appears not to be influenced by the smaller scale, proximal normal faults but rather the distant main basin bounding fault system. Perhaps, in this case, the minor fault is inactive and does not contribute to the current state of stress.

At the GA level (Fig. 5a) the borehole breakout orientations are varied and suggest two domains (divided by the dashed line) separating different stress orientations. In the southern domain, S_{hmin} directions are more or less perpendicular to the NE-SW striking main normal fault. In the northern domain the stress orientations are dominated by the more distant NW-SE striking main basin bounding growth fault (the two wells in blocks 338 and 339). We think that in these two wells the closer normal faults may be inactive and do not contribute to the state of stress. The stress orientation observed in the north of block 330 could be induced either by the small fault splay to the east of the main fault or perhaps by the salt diapir in the northeast corner of block 330. We believe these strong variations in stress orientations could be an indication of relatively low horizontal stress anisotropy.

Discussion. The results presented above show that the state of stress in the SEI field is characteristic of an active normal faulting environment, where, in general, the least principal stress is perpendicular to the main basin bounding and smaller scale normal faults. However, we can identify appreciable variations induced by either salt diapirs or relatively small horizontal stress anisotropy. In some cases, the stress orientation may reflect the influence of more distant faults because proximal faults could be inactive. Nonetheless, our results hold for three different stratigraphic levels with extremely high structural variability and are also independent of pore pressure conditions, which vary between hydrostatic and severely overpressured. This conclusion is also consistent with results from the stress analysis in the Pathfinder well[22] and with Anderson's faulting theory[26], where principal stresses in extensional regions are approximately horizontal, less in magnitude from the vertical stress, and cause active faults to slip, which are oriented more or less perpendicular to S_{hmin}.

Constraining S_{Hmax} Magnitude. We attempt to constrain the full stress tensor from wellbore failure in deviated boreholes by using specific procedures that were described in detail by Peska and Zoback[21] and Zoback and Peska[22]. Similar to the analysis in the Pathfinder well[22], we utilize borehole breakout observations in inclined wells (i.e., inclination >20) in association with pore pressure, least principal stress, and maximum principal stress measurements in order to determine S_{Hmax} magnitude. The results will also render approximate values for uniaxial compressive rock strength, C_0. Because stress magnitudes are generally different between shales and sands, we limit this study solely to

breakout observations in sand reservoirs from which we have independent and accurate pore pressure and stress data available, as described above. Two wells qualify for this analysis for which the results are summarized in **Table 1**.

Because the breakouts were observed in the same sand intervals from which we have minifrac and pore pressure history data available, we assume firstly, that within each sand reservoir the effective stress ratio between the depth of a stress/pore pressure measurement and the depth of an observed breakout is constant, and secondly, the vertical stress, S_V, is a principal stress axis. Again, this latter assumption is based on the fact that vertical fractures were detected in the core of the Pathfinder well[25] and FMI logs[22]. Hence, the problem of constraining the full stress tensor is reduced to two unknowns: the magnitude and orientation of S_{Hmax}. We obtained S_V by integrating density logs.

To constrain the full stress tensor we need a series of input parameters (see Ref. 19 and 22 for details) and assume that the minimum breakout width was at least 20° (otherwise the dipmeter tool would not have detected the breakout) and 90° at most, which corresponds to half of the wellbore's circumference that has failed in compression (any larger value would lead to a washout which we would discard from our analysis). Given these input parameters, we can constrain the full stress tensor modeling in two different ways: (1) determine ranges of maximum principal horizontal stress magnitudes and orientations; this requires the specification of a value for S_{hmin} from an independent measurement (i.e., minifrac); (2) determine ranges of S_{hmin} and S_{Hmax} magnitudes; this requires specification of stress orientation from an independent observation (i.e., from a breakout observed in a well nearby). After performing a grid search in between these different stress ranges, the models render possible stress tensor values for S_{Hmax} azimuth versus magnitude in case (1) and S_{hmin} versus S_{Hmax} magnitudes in case (2) that are consistent with the observed borehole breakouts. These results are a function of critical C_0 values for which compressive borehole failure would occur under conditions consistent with our in-situ observations.

As an example, we show in **Fig. 6** how we constrained the full stress tensor from a breakout observed in one of the two wells. Fig. 6a displays the result of a mode (1) run. Given that S_V and S_{hmin} were obtained from independent data and the assumption that the S_V is a principal stress, we can find the two missing stress components (i.e., S_{Hmax} magnitude and azimuth) in the following way: the grayish area pinches out towards 7,125 psi and S_V is an upper bound; therefore, S_{Hmax} ranges from 7,125 psi to 7,549 psi at azimuths from 145° to 170°, which constrains the full stress tensor. Effective rock strength, C_0, in this case, ranges from approximately 3,300 psi to 3,700 psi. We determined the stress tensor for the second well in a similar fashion (Table 1).

Fig. 6b displays the results from the mode (2) run. In this case, the grayish area presents possible combinations of principal horizontal stress magnitudes as a function of C_0. We can use this figure to constrain S_{Hmax} magnitude by specifying stress orientations (from a nearby well) and independently obtained S_{hmin} and S_V magnitudes (from minifrac and density log respectively). Utilizing this independent data, we can constrain a lower bound for S_{Hmax} magnitude by intersecting the dashed S_{hmin} line with the gray area. The resulting range of S_{Hmax} magnitudes is: ~ 7,180 psi to 7,300 psi. The figure also shows that S_V magnitude plots to the right of the S_{Hmax} range indicating that S_V is larger than any possible S_{Hmax} value. Likewise for the second well: S_{Hmax} ranges from ~ 6,313 psi to 6,319 psi, while S_{hmin} and S_V are 6,300 psi and 6,335 psi respectively. Hence, in both cases S_V is the maximum stress. Because we assume that S_V is a principal stress, we identify S_{Hmax} as the intermediate principal stress, S_2, and S_{hmin} as the least principal stress, S_3. The results from this figures confirms a normal faulting environment where S_V is the maximum principal stress (i.e., $S_V > S_{Hmax} > S_{hmin}$).

It is clear that S_{hmin} and S_{Hmax} values are not equal even in the severely overpressured Lentic sand. This is a particularly interesting point because it is commonly assumed that S_{hmin} equals S_{Hmax} in the Gulf of Mexico[4,5,6,7,8,27]. In fact, considering that breakouts did form in the SEI field is in itself sufficient evidence that differential principal horizontal stresses have to exist for the development of hoop stress around the wellbore; this is a necessary condition for stress induced breakouts to form. Nevertheless, the variations in the stress orientations seen at the GA level (Fig. 5a) and in other studies[28] suggest that the overall horizontal stress anisotropy is relatively small.

Conclusions

In this study, we constrain the full stress tensor in sand reservoirs of the SEI field, a typical minibasin in the Gulf of Mexico, by integrating minifrac, pore pressure history, density log, and caliper data. Analysis of least principal stress and pore pressure data show considerable pressure drawdown as a result of production. We identified a stress path for one of the reservoir sands that indicates a ratio of least principal stress change over change of pore pressure of about 0.8, which we used to restore the initial state of stress in all reservoir sands studied. Initial reservoir pore pressures and stresses show significant variability. Regardless of depletion, least principal stresses range from 80% to 99% of S_V. Pore pressures vary from near hydrostatic to severely overpressured (i.e., 48% to 95% of S_V). The effective stress ratio, K, in these reservoir sands scatters significantly and is bound by an isotropic state of stress (i.e., K = 1) and Coulomb failure for a coefficient of friction of 0.6 (i.e., K = 0.33). This indicates that while some of the sands are in frictional equilibrium, the majority show lower differential stresses than predicted by Coulomb faulting with coefficients of friction (μ) of ~0.6 (perhaps because they behave visco-elastically and dissipate differential stresses over time or μ is very low). We think that the strong variations in K may reflect interactions between stress/strain boundary conditions and material properties. Comparison with common regressions to predict fracture gradients in the Gulf Coast shows no correlation with our data or among the individual regressions. We believe, these regressions are not appropriate for prediction of fracture gradients in the SEI reservoir sands.
Results of borehole breakout analysis from caliper data indicates a stress field that is consistent with an active

extensional environment: while stress directions vary spatially in between fault blocks, S_{hmin} orientations are predominantly perpendicular to the minibasin bounding growth fault trends but show considerable scatter. Constraining the full stress tensor from borehole breakout analysis in highly inclined wells (i.e., inclination > 20°) results in stress magnitudes that confirm a normal faulting environment, where the overburden is the maximum principal stress (i.e., $S_V > S_{Hmax} > S_{hmin}$).

Nomenclature

A = stress path parameter
C_0 = uniaxial compressive rock strength, m/Lt^2, MPa
K = effective stress ratio
λ = normalized pore pressure
P_p = reservoir pore pressure, m/Lt^2, psi
S_3 = least principal stress, m/Lt^2, psi
S_{hmin} = least horizontal stress, m/Lt^2, psi
S_{Hmax} = maximum horizontal stress, m/Lt^2, psi
S_v = vertical stress, m/Lt^2, psi

Acknowledgments

We would like to thank Texaco, Shell, and Pennzoil for generously providing the data. Peter Flemings and Beth Stump from the Pennsylvania State University were invaluable in retrieving the data for this work and made many useful comments and suggestions. This project is financially supported by the Gas Research Institute under contract no. 5095-260-3558 and the Stanford Rock and Borehole Geophysics Consortium (SRB).

References

1. Alexander, L.L. and Flemings, P.B.: "Geologic evolution of a Plio-Pleistocene salt withdrawal minibasin: Eugene Island block 330, offshore Louisiana," *AAPG Bulletin* (Dec. 1995) 1737.
2. Holland, D.S., *et al.*: "Eugene Island Block 330 field - USA, offshore Louisiana," *Structural traps III, tectonic fold and fault traps*, E.A. Beaumont and N.H. Foster (eds.), Atlas of Oil and Gas Fields, AAPG Treatise of Petroleum Geology, Tulsa (1990) 103.
3. Schuhmacher, D.,: "Eugene Island Block 330 field, offshore Louisiana, geochemical evidence for active hydrocarbon recharging," *AAPG Annual Convention Program* (1993) 179.
4. Althaus, V.E., "A new model for fracture gradient," *Journal of Canadian Petroleum Technology* (Apr-Jun 1977), 98.
5. Breckels, I.M., and vanEekelen, H.A.M.: "Relationship between horizontal stress and depth in sedimentary basins," *JPT* (1982), **34**, 2191.
6. Brennan, R.M., and Annis, M.R.: "A new fracture gradient prediction technique that shows good results in Gulf of Mexico abnormal pressure," paper SPE 13210 presented at the 1984 SPE Annual Technical Conference and Exhibition, Houston, Sep. 16-19.
7. Mathews, W.R., and Kelly, J.: "How to predict formation pressure and fracture gradient," *The Oil and Gas Journal* (Feb. 1967), 92.
8. Pilkington, P.E.: "Fracture gradient estimates in Tertiary basins," *Petroleum Engineer International* (May 1978), 138.
9. Zoback, M.D., and Healy, J.H.: "Friction, faulting, and in-situ stress," *Annales Geophysicae* (1984), **2**, 689.
10. Nur, A.M., and Walder, J.: "Time-dependent hydraulics of the Earth's crust," *The role of fluids in crustal processes*, National Academic Press, Washington D.C. (1990) 113.
11. Chang, C.T., and Zoback, M.D.: "The role of viscous rheology in the state of stress of unconsolidated sands," paper SPE 47401 presented at the 1998 SPE Annual Technical Conference and Exhibition, Trondheim, Jul. 8-10.
12. Engelder, T., and Fischer, M.P.: "Influence of poroelastic behavior on the magnitude of minimum horizontal stress, Sh, in overpressured parts of sedimentary basins," *Geology* (Oct. 1994), **22**, 949.
13. Teufel, L.W. et al.: "Effect of reservoir depletion and pore pressure drawdown on in-situ stress and deformation in the Ekofisk Field, North Sea," *Rock Mechanics as a Multidisciplinary Science*, Roegiers (ed.), Balkema, Rotterdam (1991) 63.
14. Bell, J.S., and Gough, D.I.: "Northeast-southwest compressive stress in Alberta: evidence from oil wells," *Earth and Planetary Science Letters* (1979), **45**, 475.
15. Zoback, M.L., and Zoback, M.D.: "State of stress in the conterminous U.S.," *JGR* (1980), **85**, 6,113.
16. Zoback, M.D., and Zoback, M.L.: "Tectonic stress field of North America and relative plate motions," *Neotectonics of North America*, D.B. Slemmons, E.R. Engdahl, and M.D. Zoback (eds.), GSA Decade Map Volume 1, Boulder (1991).
17. Zoback, M.D. *et al.*: "Wellbore breakouts and in-situ stress," *JGR* (1985), **90**, 5,523.
18. Plumb, R.A., and Cox, J.W.: "Stress directions in eastern North America determined to 4.5km depth from borehole elongation measurements," *JGR* (1987), **92**, 4,805.
19. Zoback, M.L. *et al.*: "Global patterns of intraplate stresses; a status report on the world stress map project of the International Lithosphere Program," *Nature* (1989), **341**, 291.
20. Zheng, Z. *et al.*: "Analysis of borehole breakouts," *JGR* (1989), **94**, 7,171.
21. Peska, P., and Zoback, M.D.: "Compressive and tensile failure of inclined wellbores and determination of in-situ stress and rock strength," *JGR* (1995), **100**, 12,791.
22. Zoback, M.D., and Peska, P.: "In-situ stress and rock strength in the GBRN/DOE Pathfinder well, South Eugene Island, Gulf of Mexico," *JPE* (1995) 582.
23. Plumb, R.A., and Hickman, S.H.: "Stress-induced borehole elongation: a comparison between the four arm dipmeter and the borehole televiewer in the Auburn geothermal well," *JGR* (1985), **90**, 5,513.
24. Mastin, L.: "Effect of borehole deviation on breakout orientation," *JGR* (1988), **93**, 9,187.
25. Losh, S.: "Oil migration in a major growth fault: structural analysis of the Pathfinder core, South Eugene Island Block 330, offshore Louisiana," in press.
26. Anderson, E.M.: "The dynamics of sheet intrusion," *Proc. R. Soc. Edinburgh* (1937), **58**, 242.
27. Daines, S.R.: "Prediction of fracture pressures for wildcat wells," *JPT* (April 1982) 863.
28. Yassir, N.A., and Zerwer, A.: "Stress regimes in the Gulf Coast, offshore Louisiana: data from well-bore breakout analysis," *AAPG Bulletin* (Feb. 1997), **81**, 293.

SI Metric Conversion Factors

Mpa × 1.450	E + 02 = psi
ft × 3.048	E - 01 = m

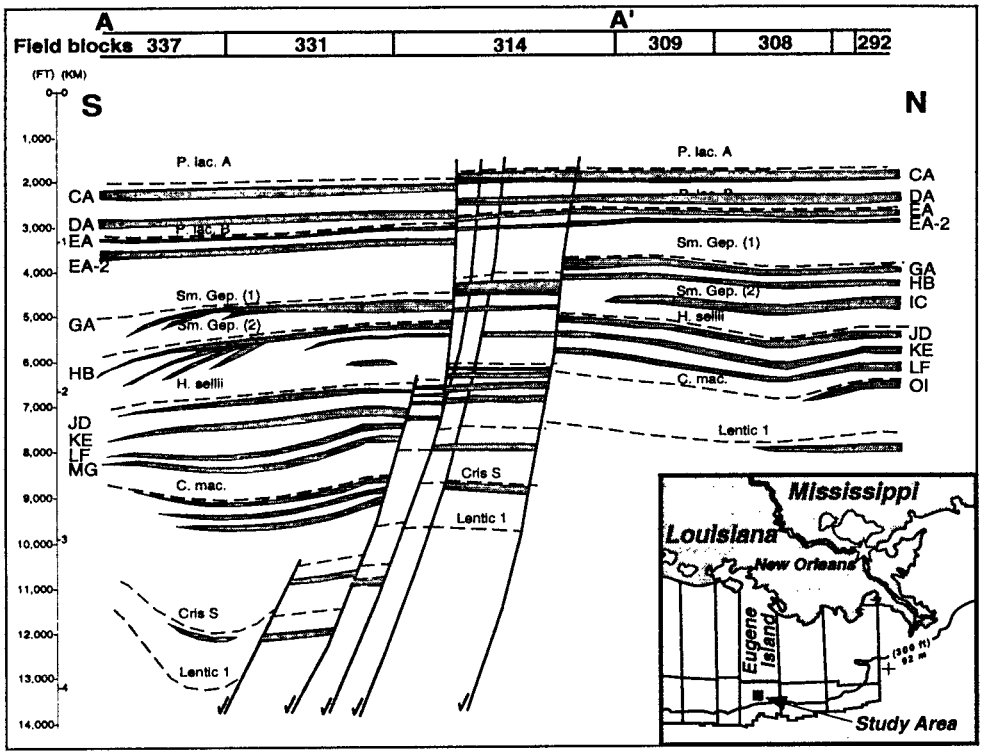

Fig. 1–Cross-section through the SEI field along transect A-A' shown in Fig. 5. Reservoir sands are displayed in gray, labeled with their names. Dashed lines are corresponding flooding surfaces (modified from Alexander and Flemings, Ref. 1). The inset helps to locate the field in the Gulf of Mexico.

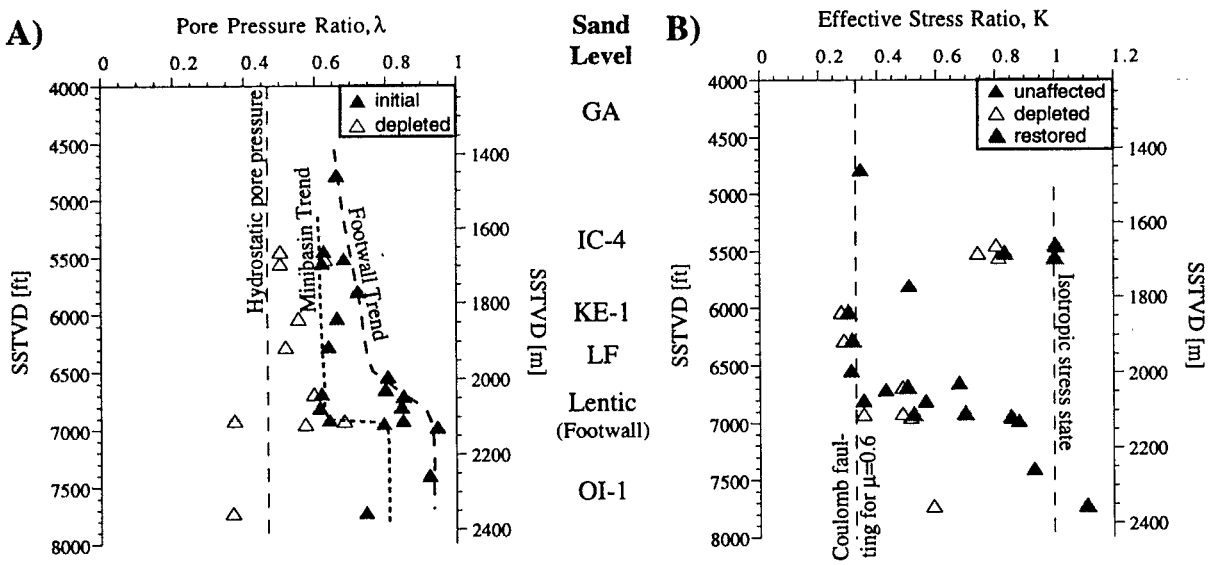

Fig. 2–A) Normalized pore pressure (λ=Pp/Sv) versus SSTVD (sub-sea true vertical depth) for depleted (open triangles) and initial (solid triangles) conditions. The three dashed lines show the following pore pressure trends: 1) hydrostatic (for reference), 2) minibasin (initial conditions), and 3) footwall (initial conditions). B) Effective stress ratio, K, versus SSTVD for depleted (open triangles) and initial conditions. "Unaffected" refers to negligible pore pressure drawdown (black triangles) and "restored" to appreciable pore pressure drawdown (gray triangles) data. The two dashed lines show the bounds for Coulomb frictional faulting (K=0.32) and isotropic stress state (K=1) respectively.

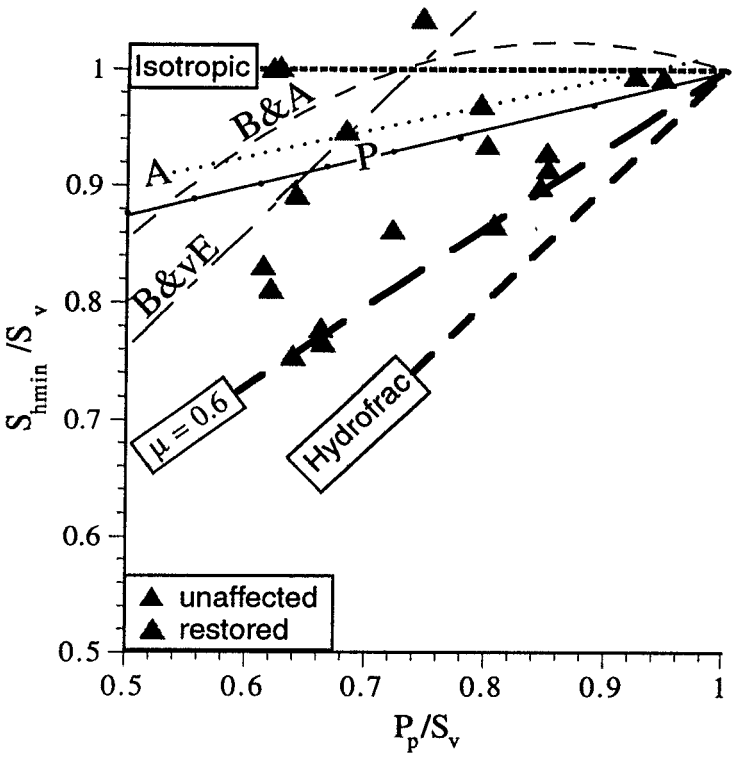

Fig. 3–Normalized least principal horizontal stress versus normalized pore pressure. We display initial conditions only (black and gray triangles, refer to Fig. 2b). Hydrofrac, frictional faulting, and isotropic stress state lines are shown dashed. The four different fracture gradient regressions were calculated for a reference depth of 6500 ft. and an average overburden gradient of 0.92 psi/ft. A: Althaus (Ref. 4); B&vE: Breckels and van Eekelen (Ref. 5); B&A: Brennan and Annis (Ref. 6); P: Pennzoil (unpublished data).

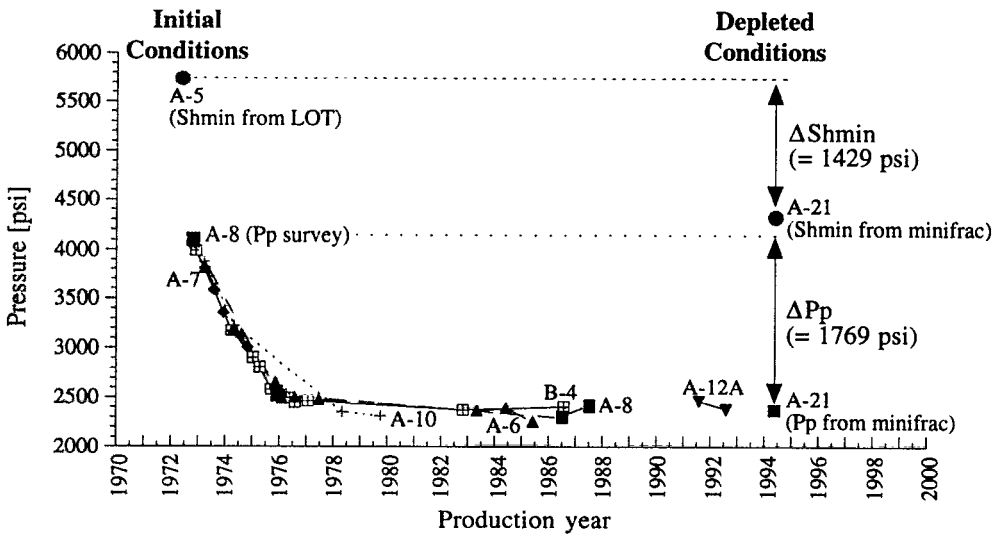

Fig. 4–Pore pressure history from pressure surveys in 7 wells (labeled) and least principal stress data (LOT and minifrac) from two wells (labeled) drilled into one of the SEI reservoir sands. The pore pressure data were corrected to a datum of 6911 ft. SSTVD. Note the uniform pressure decline in this reservoir suggesting a continuous compartment. For reference, we also show the hydrostatic pore pressure.

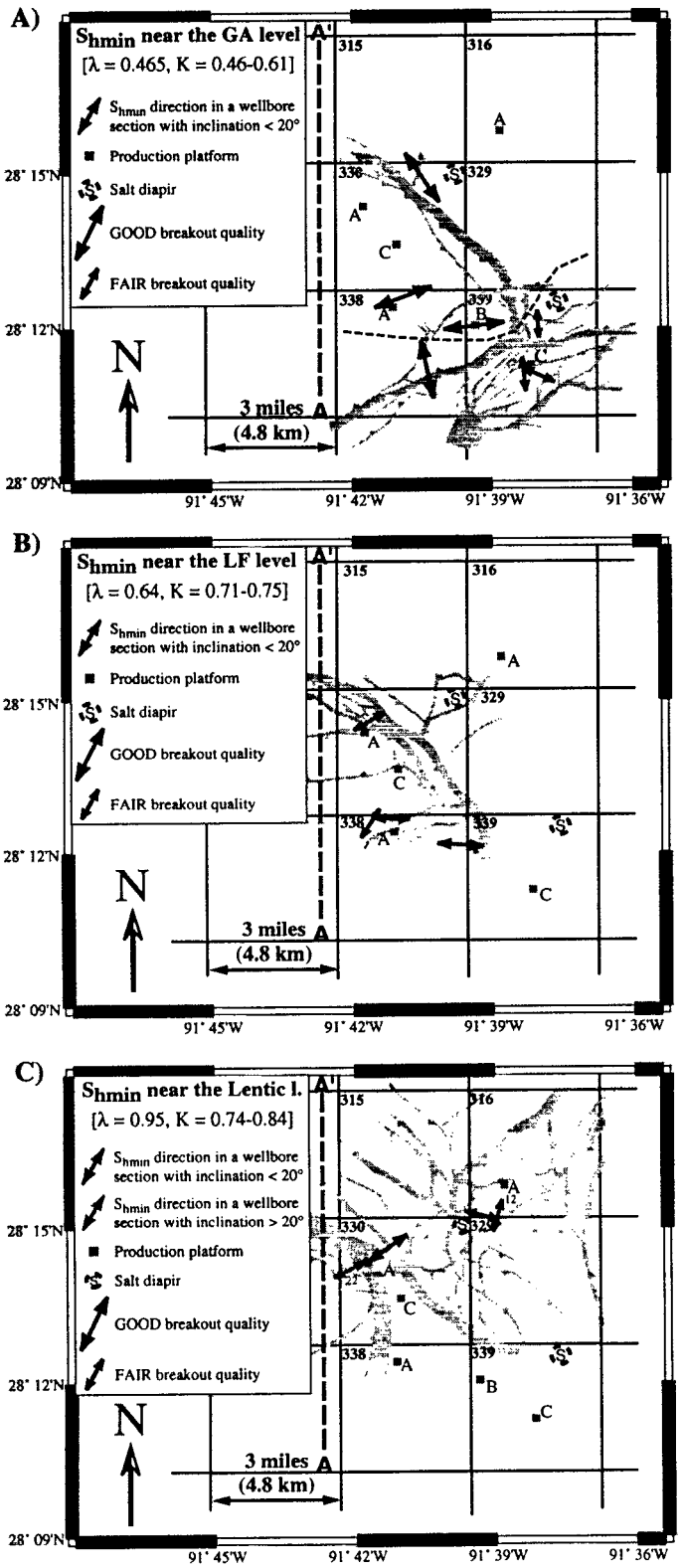
A)
Shmin near the GA level
[λ = 0.465, K = 0.46-0.61]
Shmin direction in a wellbore section with inclination < 20°
Production platform
Salt diapir
GOOD breakout quality
FAIR breakout quality
N
3 miles
(4.8 km)
A'
315
316
329
338
339
28° 15'N
28° 12'N
28° 09'N
91° 45'W
91° 42'W
91° 39'W
91° 36'W
B)
Shmin near the LF level
[λ = 0.64, K = 0.71-0.75]
Shmin direction in a wellbore section with inclination < 20°
Production platform
Salt diapir
GOOD breakout quality
FAIR breakout quality
N
3 miles
(4.8 km)
A'
315
316
329
338
339
28° 15'N
28° 12'N
28° 09'N
91° 45'W
91° 42'W
91° 39'W
91° 36'W
C)
Shmin near the Lentic l.
[λ = 0.95, K = 0.74-0.84]
Shmin direction in a wellbore section with inclination < 20°
Shmin direction in a wellbore section with inclination > 20°
Production platform
Salt diapir
GOOD breakout quality
FAIR breakout quality
N
3 miles
(4.8 km)
A'
315
316
328
330
338
339
28° 15'N
28° 12'N
28° 09'N
91° 45'W
91° 42'W
91° 39'W
91° 36'W

Fig. 5–Structuremaps of the GA, LF, and Lentic sand levels displaying Shmin directions resulting from the borehole breakout observations. We only display fair and good quality data. Derivation of stress direction in the two highly inclined wells (gray arrows) is described in detail in a later section. Dashed line A-A' marks the transect of the cross-section from Fig. 1. The curved dashed line in (A) displays the two domains (i.e., north and south) as motivated by the stress orientations at this structural level.

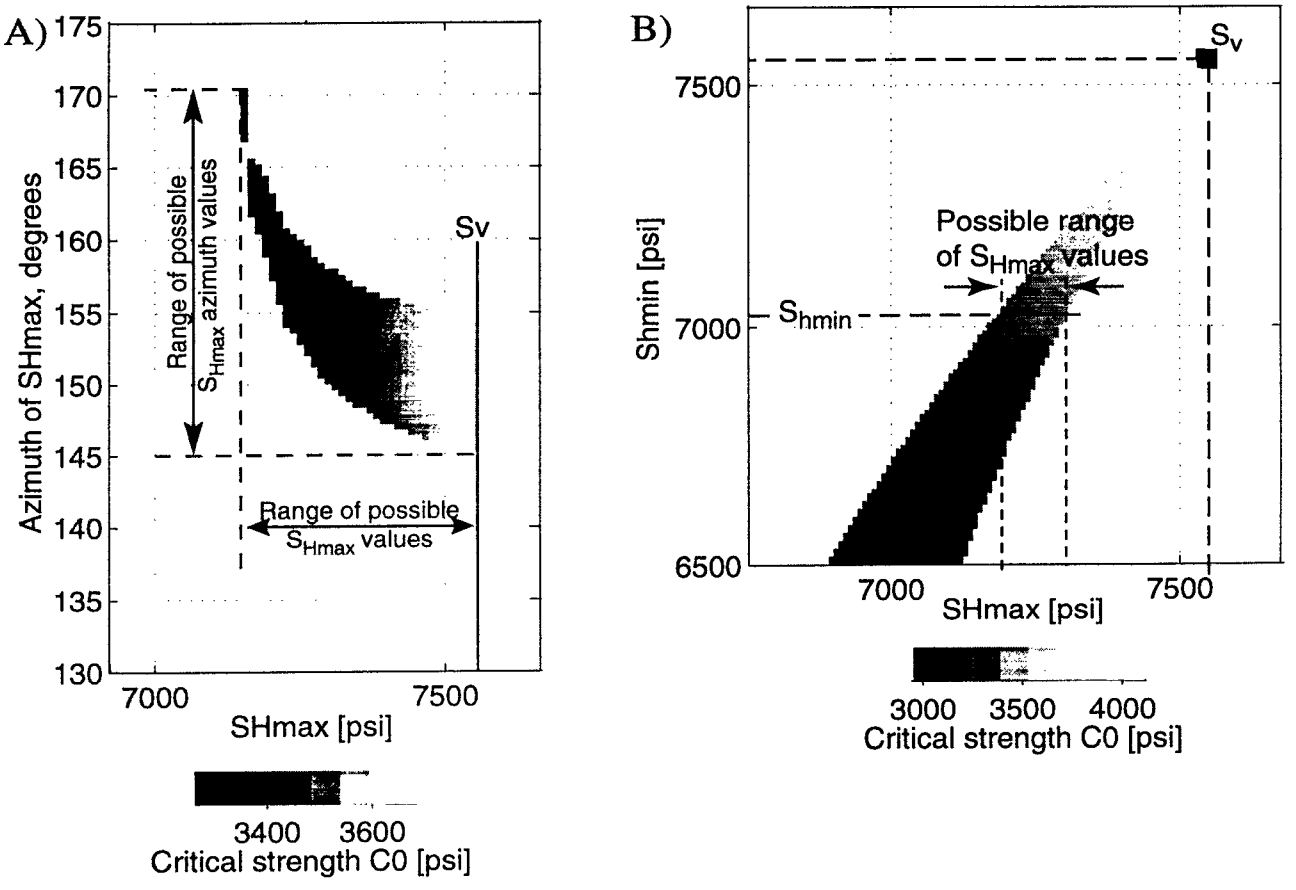

Fig. 6–Constraining the full stress tensor consistent with breakout occurrence and in-situ pore pressure and stress conditions in well 330/A-22 near the Lentic sand. The well was drilled at an azimuth of N261°E and deviated from the vertical by 23°. The annotated values for Shmin and Sv come from independent measurements and provide lower and upper bounds respectively to determine SHmax magnitude and orientation. We assume that the coefficient of internal friction is 1.0, Poisson's ratio is 0.25, and the breakout width is 90°. A) Resulting ranges of SHmax magnitudes and orientations and associated compressive strength values, C0. B) Resulting SHmax magnitude and associated compressive strength values, C0.

TABLE 1 - RESULTS FROM CONSTRAINING THE FULL STRESS TENSOR

Well	Nearest Reservoir	Available Shmin Measurement			At Observed Breakout Depth					Constr. the Stress at BO Depth		
		Type	SSTVD [ft]	K	SSTVD [ft]	Pp [psi]	Sv [psi]	λ	S_{hmin} [psi]	S_{Hmax} [psi]	S_{hmin} orient.	C_0 [psi]
316/A-12	Lentic	Minifrac	6985	0.82	6985	6137	6335	0.96	6300	6315	N190E	350
330/A-22	Lentic	Minifrac	7727	0.73	8116	5519	7549	0.73	7018	7250	N67E	3350